Automatic Offline-Capable Smartphone Paper-Based Microfluidic Device for Efficient Alzheimer's Disease Detection

Sixuan Duan1,2,3 , Tianyu Cai1 , Fuyuan Liu1,2, Yifan Li1,2, Hang Yuan1 , Wenwen Yuan1,2,4 , Kaizhu Huang5 , Kai Hoettges2 , Min Chen1,2, Eng Gee Lim1,2, Chun Zhao1,2 , and Pengfei Song1,2*

1 School of Advanced Technology, Xi'an Jiaotong-Liverpool University, 111 Ren'ai Road, Suzhou, China, 215000

2 Department of Electrical and Electronic Engineering, University of Liverpool, Foundation Building, Brownlow Hill, Liverpool, UK, L69 7ZX

3 Key Laboratory of Bionic Engineering, Jilin University, 5988 Renmin Street, Changchun, China, 130022

4 State Key Laboratory for Manufacturing Systems Engineering, Xi'an Jiaotong University, No.28 Xianning West Road, Xi'an, China, 710079

5 Department of Electrical and Computer Engineering, Duke Kunshan University, 8 Duke Avenue, Kunshan, China, 215316

*Corresponding author:pengfei.song@xjtlu.edu.cn; +86-0512-8188-9039.

Abstract

Background: Alzheimer's disease (AD) is a prevalent neurodegenerative disease with no effective treatment. Efficient and rapid detection plays a crucial role in mitigating and managing AD progression. Deep learning-assisted smartphone-based microfluidic paper analysis devices (µPADs) offer the advantages of low cost, high sensitivity, and rapid detection, providing a strategic pathway to address large-scale disease screening in resource-limited areas. However, existing smartphone-based detection platforms usually rely on large devices or cloud servers for data transfer and processing. Additionally, the implementation of automated colorimetric enzyme-linked immunoassay (c-ELISA) on µPADs can further facilitate the realization of smartphone µPADs platforms for efficient disease detection. Results: This paper introduces a novel deep learning-assisted offline smartphone platform for early AD screening, offering real-time monitoring and rapid detection in low-resource areas. The proposed platform features a simple mechanical rotating structure controlled by a

smartphone, enabling fully automated c-ELISA on μPADs. Our platform successfully applied sandwich c-ELISA for detecting the β-amyloid peptide 1-42 (Aβ 1-42, a crucial AD biomarker) and demonstrated its efficacy in 38 artificial plasma samples (healthy: 19, unhealthy: 19, N=6). Moreover, we employed the YOLOv5 deep learning model and achieved an impressive 97% accuracy on a dataset of 1824 images, which is 10.16% higher than the traditional method of analyzing curve-fitting results. The trained YOLOv5 model was seamlessly integrated into the smartphone using the Ncnn convolutional neural network (NCNN) framework, enabling deep learning-assisted offline detection. A user-friendly smartphone application was developed to control the entire process, realizing a streamlined "samples in, answers out" approach. Significance: This deep learning-assisted, low-cost, user-friendly, highly stable, and rapid-response automated offline smartphone-based detection platform represents a significant advancement in point-of-care testing (POCT). Moreover, our platform provides a feasible approach for efficient AD detection, particularly in areas with low resources and limited communication infrastructure.

Keywords: Smartphone-based; Offline; Microfluidic paper analysis devices (μPADs); Deep learning; Colorimetric enzyme-linked immunoassay (c-ELISA); Alzheimer's disease.

Introduction

Alzheimer's disease (AD) is an irreversible neurodegenerative disease without effective therapeutic drugs or treatments to date [1, 2]. Efficient and rapid detection emerges as crucial strategies to impede and manage AD progression [3-5]. Conventional methods such as magnetic resonance imaging (MRI) and positron emission computed tomography (PET) are not suitable for large-scale applications, especially in resource-limited areas [6-8]. Cerebrospinal fluid biomarker tests are not widely used due to their technical expertise and invasive nature [9-11]. Therefore, blood biomarker testing has received widespread attention thanks to its advantages of low cost and ease of detection [12-14]. Recent studies have demonstrated that the detection of plasma biomarkers of β-amyloid 1-42 (Aβ 1-42) is highly effective in AD detection [15-17]. This breakthrough highlights the potential for blood biomarker testing in efficient and rapid AD detection as a key solution for resource-limited settings.

Point-of-care testing (POCT), celebrated for its high sensitivity, rapid detection, and cost-effectiveness, provides a strategic avenue to address healthcare challenges in resource-limited settings [18-20]. This approach allows for effective real-time screening and detection of diseases directly at patient sites, outperforming traditional lab-based methods in terms of speed and accessibility. Provides a new method for screening AD. Microfluidic paper-based analytical devices (μPADs) have gained prominence as a promising platform for POCT due to their low cost, ease of

operation, and independence from external power requirements [21-23]. While various immunoassays, including electrochemical, chemiluminescent, and fluorescent immunoassays, have been successfully developed on μPADs, colorimetric enzymelinked immunosorbent assays (c-ELISA) stand out as the gold standard for detecting protein biomarkers in disease-related clinical samples, and its results can be easily and directly analyzed through color change [24-28]. However, conventional c-ELISA requires complex manual operations, including repetitive addition of reagents and analysis of results. At the same time, professionals need to wait for the previous reaction to complete before manually performing the next step, ultimately leading to lower reproducibility and efficiency. These limitations have hindered the widespread use of c-ELISA methods in the POCT setting. Therefore, to solve complex manual operations, we propose the μPAD with a simple mechanical rotary structure, where the reagents required for testing are stored in the μPAD, and only a mechanical control structure is required to automate the testing.

The popularity and portability of smartphones have led to their widespread use in various sensing techniques, especially for colorimetric detection. Smartphones incorporate the essential capabilities necessary for typical biosensing, such as cameras for signal capture, screens for signal display, and operating systems for creating graphical user interfaces to analyze the acquired data [29, 30]. Especially when combined with deep learning, it is expected to increase its sensitivity as a biosensor and simplify the detection process [31-35]. In recent years, deep learning has played a crucial role in POCT detection, analysis, and diagnosis thanks to its ability to directly, automatically, accurately, and quickly assist biosensor readings. Particularly in the classification problem of image results for biosensors, the deep learning model can remove the influence of external adverse conditions and can automatically extract useful features from the number of noisy and low-resolution raw images that overlap each other severely and obtain reasonable analysis results [36, 37]. Devices commonly used for deep learning result prediction include 1) large computing devices. 2) cloud server. and 3) sensor detection devices. The first two methods need to transmit the detection data to the large-scale equipment or the cloud, and then return the prediction results to the sensor detection equipment. The third method can directly port the trained model to the sensor detection device for direct result prediction. This approach is necessary in regions or remote mountainous areas that lack large computing devices and underdeveloped network connections [38]. However, most of the existing deep learning-assisted smartphone detection uses the first two prediction devices [29-35]. Therefore, to meet the requirements of resource-poor regions and achieve fast, sensitive, and low-cost detection, we port the trained deep model to the smartphone side to achieve offline smartphone local detection. Meanwhile, our development of the fully automated μPAD c-ELISA platform further promotes the smartphone as a biosensor.
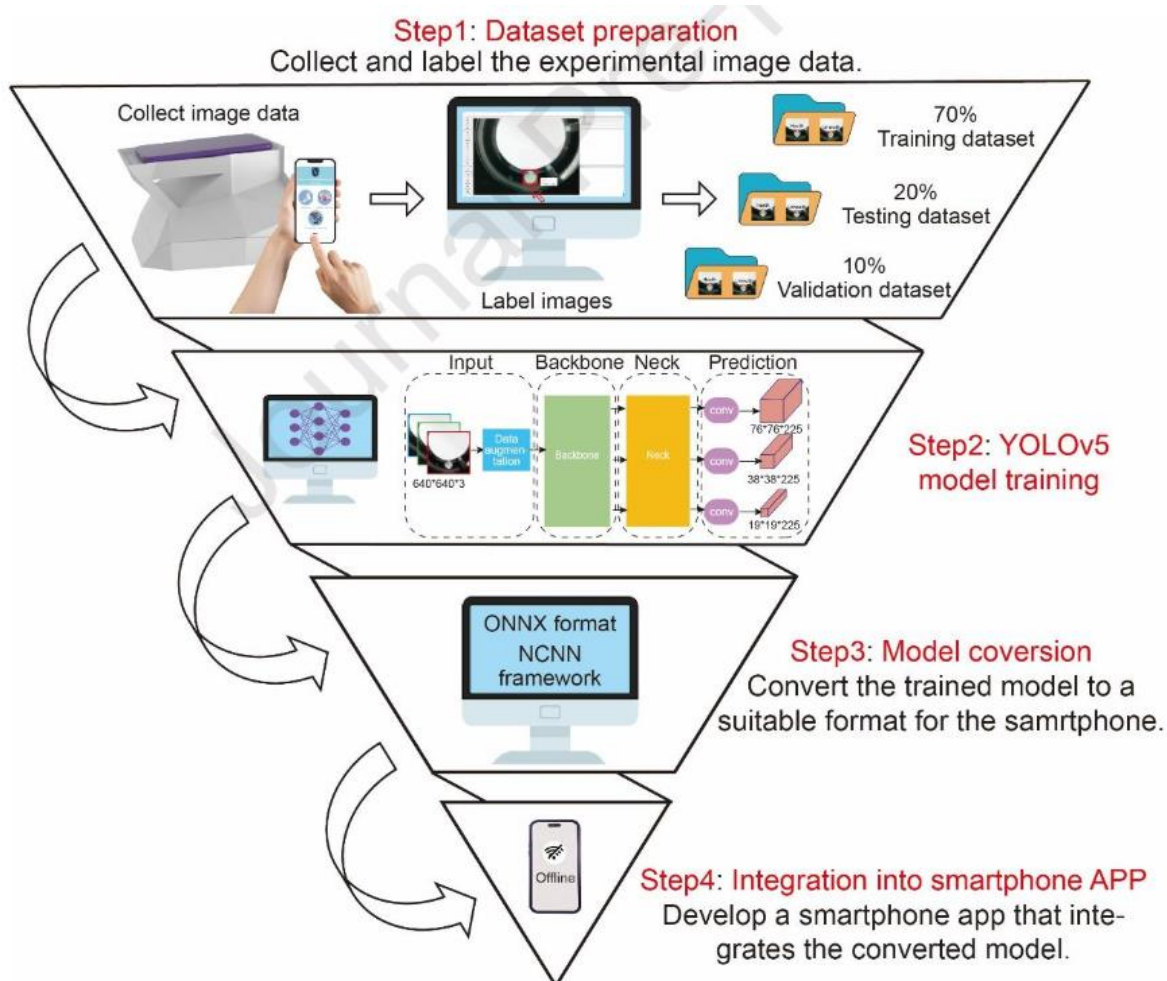
In this paper, we present a deep learning-assisted smartphone platform for fully automated μPAD c-ELISA detection. The platform has two notable features: 1) It enables offline smartphone detection without the requirement of large computing devices or cloud data transfer. This feature facilitates real-time monitoring and rapid detection, which is particularly beneficial in areas with limited communication infrastructure. It promotes the development of smartphones as biosensors. 2) A simple mechanical rotary structure is used to achieve a highly stable and rapid fully automated immunoassay, reducing the complexity of manual operation. The platform we developed has been successfully applied to complex sandwich c-ELISA for the detection of artificial plasma Aβ 1-42 samples, enabling efficient AD detection. In addition, to train the deep learning YOLOv5 model, we used different smartphones to capture the resulting images, generating a final image dataset. The YOLOv5 model provides a higher accuracy than traditional curve-fitting result analysis methods. Finally, a user-friendly smartphone APP was developed to control the whole process, and the YOLOv5 model will deploy using the Ncnn convolutional neural network (NCNN) framework, realizing offline "samples in, answer out". Our platform provides a feasible approach for effective large-scale detection of disease, furthering the development of smartphones as biosensors in the POCT field.

Experimental section

Material and reagent preparation

The supplementary information contains a detailed list of the reagents and materials used in the experiment. To simulate real AD samples, we referred to the research work by Shieh-Yueh Yang et al. from 2017, which utilized the high-Tc superconducting-quantum-interference-device based immunomagnetic reduction (IMR) quantification to detect the Aβ 1-42 protein in human plasma samples and provided a cut-off value of 16.42 pg mL-1 [16]. Based on the defined cut-off value, our experiment comprised the creation of 38 artificial plasma samples, divided into 19 healthy and 19 unhealthy samples. Aβ 1-42 peptide solution at a concentration of 16.42 pg mL-1 was first prepared in artificial plasma at 380 ul and distributed evenly into 38 microcentrifuge tubes. Following this, to simulate unhealthy samples, a random volume of Aβ 1-42 peptide was added to 19 tubes. In contrast, the remaining 19 tubes were augmented with a comparable volume of artificial plasma, representing healthy samples. This approach produced 38 samples with unspecified concentrations, effectively mirroring the complexity and variability of clinical samples. Artificial samples have been used in several studies to verify the feasibility of their experimental methods [39, 40]. In this work, we validated the feasibility of an offline fully automated detection on a smartphone μPADs platform using artificial plasma samples as a c-ELISA sensing target with the assistance of deep learning. In future work, we will apply this platform to clinical samples.

Development of offline smartphone-based detection

Fig. 2. The schematic diagram of the process for implementing offline smartphone-based platform detection.

Offline detection on smartphones can eliminate the requirement for large-scale computing devices during each testing session and address the issue of privacy leakage in cloud data transmission. It further facilitates the development of POCT in resource-limited areas and extreme environmental conditions. For this purpose, we first selected a small deep learning model (YOLOv5) which is suitable for analyzing the c-ELISA image dataset, and then we converted the trained deep learning network into a format adapted to smartphones and deployed it on the smartphone platform using the NCNN framework. The schematic diagram of the process for implementing offline smartphone-based platform detection is shown in Fig. 2.

Specifically, for training the deep learning model to recognize the detection results of c-ELISA, we first performed the construction of the dataset. The details of the specific dataset construction are

mentioned in the following section. Furthermore, for the deep learning model to directly localize the detection region, we labeled the constructed dataset with the help of the annotation tool LabelImg. Then, 70% of the data is used for deep learning model training, 20% of the data is used as a test dataset for the deep learning model, and the remaining 10% is used to validate the generalizability of the deep learning model, tune the hyper-parameters, and prevent the occurrence of overfitting events. In addition, the YOLOv5 model is highly popular in image detection thanks to its efficiency, real-time, adaptability, and ease of use [41, 42]. Therefore, we select the YOLOv5 deep learning model to train the dataset. The structure of the YOLOv5 model is described in the following section. After the YOLOv5 model is well-trained, it needs to be converted to an open neural network exchange (ONNX) format to port this model to a smartphone. After that, it is implanted into a developed Android application using the NCNN framework [43]. Hence, the YOLOv5 deep learning model can achieve efficient and accurate detection on the smartphone, even in the absence of a network connection.
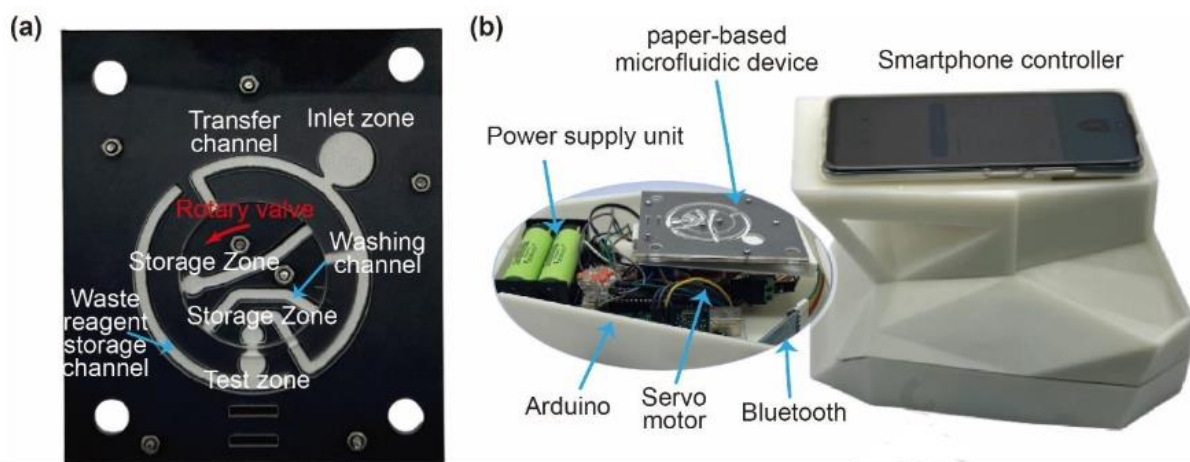
Fabrication of smartphone-based µPAD platform

Fig. 3. The photograph of the smartphone-based µPAD platform. (a) The photograph of µPAD with rotary valve. (b) The platform for integrating the µPAD with a smartphone.

To realize the automated detection of sandwich c-ELISA, we achieved a rapid and easily assembled fully automated µPAD platform through a single, straightforward mechanical rotation structure. Additionally, we employed a smartphone to control the entire experimental process and analyze the experimental results. Fig. 3(a) illustrates the physical design of the µPAD. The details of the fabrication of µPAD with a rotary valve can be found in supplementary information. Specifically, to detect the Aβ 1-42 protein in artificial plasma samples. All reagents required for the sandwich c-ELISA Aβ 1-42 protein detection are pre-stored in the storage area (TMB substrate, HRP-conjugated Aβ 1-42 antibody) and the test area (Aβ 1-42 antibodies), which are connected via paper rotary valves.

Furthermore, our μPAD features a region designated for buffer solution addition, channels facilitating reagent transport, and a compartment for waste storage.

To address the problem of reagent leakage, we optimized the parameters of the μPAD in our previous work [44]. The width of the overlap between the rotary valve and the paper sheet determines the success rate of the fluid to flow smoothly through. If the width is too small, the fluid will not be able to cross the boundary; if it is too large, leakage will occur. We tested different overlap widths and finally chose a 2 mm overlap width, which resulted in a 100% success rate of fluid passage. Meanwhile, to address the problem of reagent contamination, we designed the μPAD to have a separate storage area for each reagent. At the start of the assay, PBS buffer will sequentially transport pre-stored reagents from the storage zone to the test zone along the flow path on the μPAD. Excess reagents are stored in a pre-designed waste reagent storage channel.

Additionally, for the comprehensive control of the experiment and subsequent result analysis, we formulated a portable smartphone-based platform, complemented by a deep learning model. The platform encompasses three key constituents: (i) a μPAD employed for performing sandwich c-ELISA detection (The structure of μPAD can be found in Fig. S1.); (ii) a microcontroller comprising a servo, microcontroller unit, Bluetooth capability, and a power supply unit, dedicated to controlling the μPAD; and (iii) a smartphone engaged in overseeing the Bluetooth interface of the platform, facilitating automated sandwich c-ELISA execution and result analysis assisted by deep learning. A visual representation of the smartphone-based automatic μPAD platform is depicted in Fig. 3(b). And to make the platform design more aesthetic and ergonomic structure. We added some angles and bevels to the platform design. Further information regarding the fabrication process of the smartphone-based platform is available in the supplementary materials.

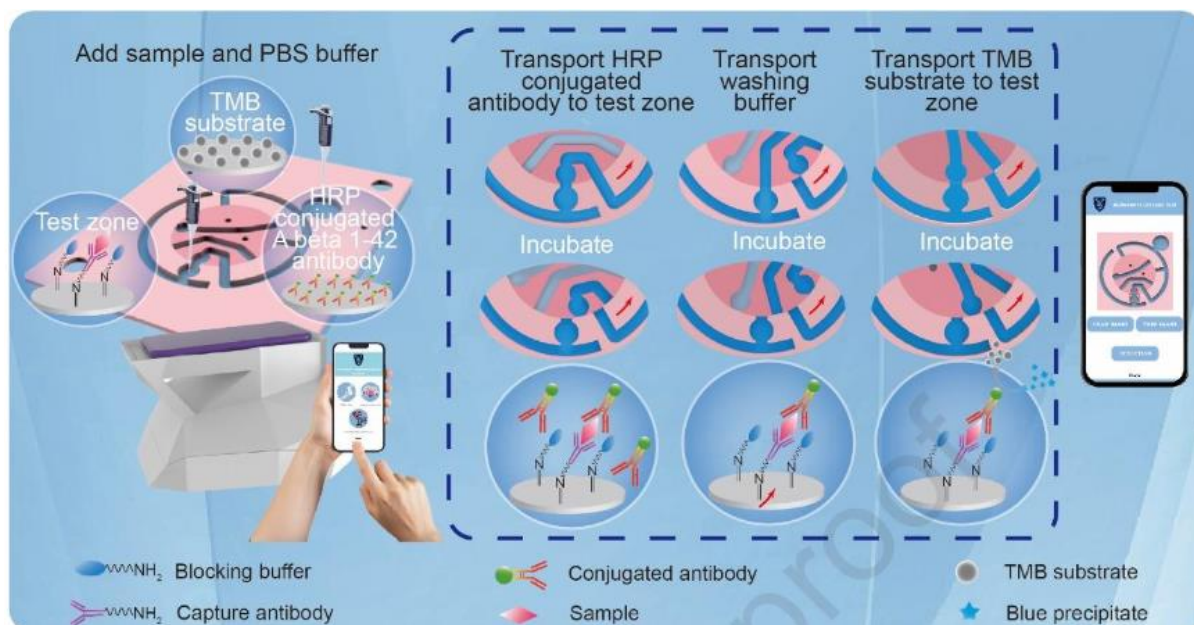Working principle of the smartphone-based platform

Fig. 4. Schematic of the workflow for detecting Alzheimer's disease (AD) via the offline smartphone platform.

To perform the AD detection by the automated smartphone-based platform, all reagents required for the sandwich c-ELISA Aβ 1-42 protein detection are pre-stored in the storage zone. Before we start the test, we first click on the Bluetooth button on the smartphone, which is used to connect the Arduino to control the servo motor to drive the paper-based rotary valve. Then, we open the platform add 3 μl artificial plasma sample to the μPAD test zone, and then drop the prepared 250 μl of 1× PBS buffer into the inlet zone. After completing the addition of the sample and PBS buffer, close the platform and place the phone on top of the platform.

By clicking the Start button on the smartphone, the paper-based rotary valve will execute in a pre-set sequence (according to the sandwich c-ELISA protocol) and the PBS buffer will follow the flow path on the μPAD, sequentially transporting the prestored reagents from the storage zone to the test zone. Specifically, the HRPconjugated Aβ 1-42 antibody is first transferred by PBS buffer to the test zone for binding to the Aβ1-42 peptide in the sample. Then, the first storage zone is disconnected from the test zone by a rotary valve control for incubation and drying. The washing channel is connected to the test zone and unbound HRP-conjugated Aβ 1-42 antibody is removed using PBS buffer. The rotary valve control channel is disconnected, incubated, and dried. Rotate the rotary valve to transfer the TMB substrate through the PBS buffer to the test zone, which reacts with the HRP-bound Aβ 1-42 antibody to form a blue precipitate. Here, we refer to previously published papers for the volume of reagents and incubation times used [18, 27, 44].

After the test, click the Take Image button on the smartphone screen and the image of the detection result will be displayed on the smartphone screen. Finally, by clicking on the Detect button, the results of the assay analysis will be automatically analyzed by a trained model and displayed on the smartphone screen. Fig. S2 illustrates the smartphone app interface operation flow. We also provided a video demonstration of the experiment in the supporting materials to further illustrate the working principle of the smartphone-based platform.

Constructing datasets for training the deep learning model

Under fixed lighting conditions, the image capture results are affected by smartphone camera resolution, aperture, focal length, etc. To improve the generalization of the deep learning model to different smartphone cameras, we used eight smartphones with different models from popular brands to capture the images (the properties of the smartphones as shown in Table S1). When acquiring the resultant image, the smartphone was taken at an angle parallel to the µPAD, and it was set to the default mode, which further minimized user intervention. In addition, the distance between the µPAD and the camera is 7 cm.

In this paper, 38 artificial plasma samples were prepared, including 19 healthy and 19 non-healthy samples. Each sample concentration was tested six times (N=6), subsequently, the results of the testing area were image captured using each smartphone, and a total of 48 images were generated for each sample. We standardized the image results for all samples into JPEG format, resulting in a training dataset with 1824 result images. The details of the construction of the training dataset results for different smartphones are shown in Table S2.

After constructing the dataset, labeling data is an important step in performing the training of the deep learning model.[45, 46] Specifically, labeling is the association of input data with corresponding labels (healthy, and unhealthy labels in this work), which are used to indicate which features should be learned by the deep learning model during the training process. In this study, we used the commonly used labeling software to draw bounding boxes for the detected regions in the resultant images and labeled their categories to form the dataset. And we defined the results of healthy samples as class 0 and unhealthy samples as class 1. After that, 70% of the labeled dataset is used for training, 20% for testing, and the rest for validation.

The structure of the YOLOv5 model

For achieving image classification of healthy and unhealthy samples, we selected the YOLOv5 deep learning model to train the dataset. YOLOv5 deep learning model is widely used in mobile devices with limited memory and computational resources (e.g., smartphones) thanks to its efficient and lightweight features. Therefore, this work applied the YOLOv5 model to train the dataset. The

YOLOv5 model mainly consists of four parts: Input, Backbone, Neck, and Head. Here, the size of the input image is 640⊆640 pixels. To avoid overfitting the model and to improve the robustness of the model, a data argumentation is added to the input module. Data augmentation can increase the amount of data for deep learning model training and improve the generalization ability and robustness of the model. Commonly used data augmentation for the YOLOv5 model includes HSV augmentation, geometric transformation (translation, scaling, rotation, shear, perspective), mosaic, and Mixup [47, 48]. In this work, we applied HSV argumentation, geometric transformation, and mosaic data augmentation. Among them, HSV (Hue, Saturation, Value) is a commonly used color representation, HSV augmentation is the maximum percentage of an image's hue, saturation, and value that can be increased or decreased from the original values. The parameters used in our model structure are 0.015, 0.7, and 0.4. In addition, translation and scaling data argumentation are also used in our model. In our work, the translation value of 0.1 indicates that the maximum translation ratio allowed is 10% of the image width or height. In addition, the translation transformation prevents the model from being affected by changes in the position of the detection target. The value of scale in our model is 0.5, which indicates that the maximum allowable scale is 50% of the original size of the image, and this scaling method can avoid over-learning of the image size by the model. Mosaic data augmentation is performed by randomly selecting 4 images from the training dataset, then randomly scaling, cropping, and arrangement, and finally, normalization is performed. In our model, the mosaic parameter is 1.0, which indicates that mosaic data augmentation will always be applied during data augmentation.

Moreover, further enhancement of the dataset improves the generalization ability of the model and further avoids sample imbalance. The main role of the Backbone part is to extract the features of the image and continuously reduce the feature images. The Neck structure is mainly designed to achieve the fusion of shallow features of the image and deep semantic features. In the shallow layer of the convolutional neural network, the network extracts some simple features such as color, contour, texture, and shape, which belong to features of the image. As the network continues to deepen, the neural network will continuously fuse and up-dimension these features to produce new features, that belong to semantic features. Moreover, YOLOv5 prediction output is 255x19x19, 255x38x38 and 255x76x76 feature images. Among them, the smallest size 255x19x19 is responsible for detecting large targets, 255x38x38 is suitable for detecting medium targets, and the largest size 255x76x76 is relevant for detecting small targets.

Results and discussion

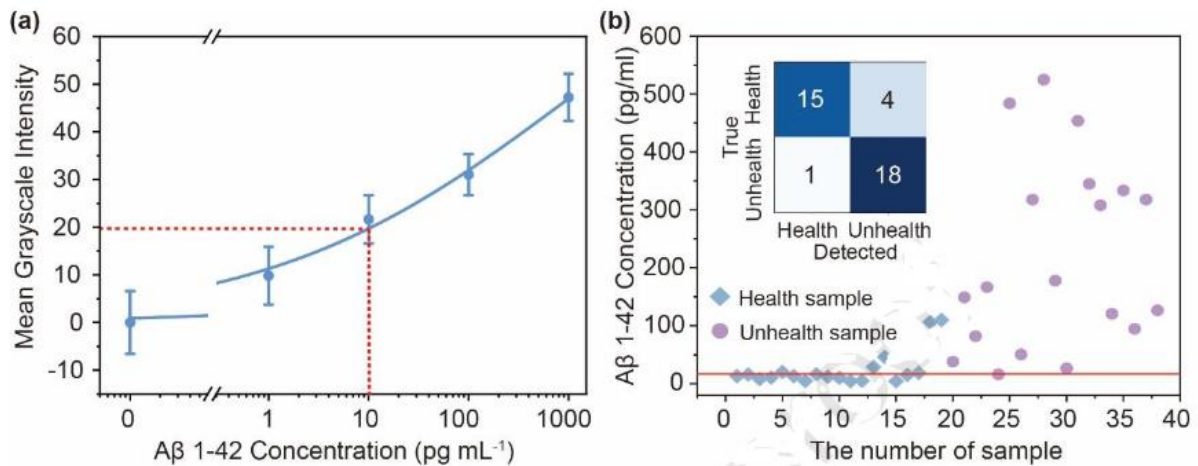The results of artificial plasma sample detection by the platform

Fig. 5. Automatic sandwich c-ELISA results of Aβ 1-42 peptide in artificial plasma. (a) Calibration curve of the mean grayscale intensity versus the Aβ 1-42 concentration (N=6). (b) The results of the traditional analytical method (manual analysis using ImageJ) for 38 random Aβ 1-42 peptide concentration samples.

 In this paper, we first carried out automatic sandwich c-ELISA for the detection of Aβ 1-42 peptide in artificial plasma on our platform. We prepared four different concentrations (N = 6 for each concentration) in 10-fold dilutions (1 pg mL -1 – 1000 pg mL-1) of Aβ 1-42 peptide as the sensing target for c-ELISA, and the artificial plasma without Aβ 1-42 peptide (0 pg mL-1) was used as a negative control. After each test, we captured an image of the test zone after each assay with a smartphone (iPhone 11). We measured the average grayscale intensity of all test zones by ImageJ. Then, the intensity data were fitted using the Hill equation (Fig. 5(a)) for the sigmoidal curve (s-curve), and the limit of detection (LOD) and coefficient of determination (COD, denoted as R2) were calculated [18]. The LOD is determined by using the 3σ of the lowest concentration sample (0 pg mL-1) with a value of 10.07 pg mL-1 and the COD (COD = 0.994) represents the strength of a curve fitting, and the better the curve fit, the closer the value of COD is to 1.

In addition, we tested 38 artificial plasma samples, including 19 healthy samples and 19 non-healthy samples. We uniformly used an iPhone 11 smartphone to capture the images of the test results and measured the average gray intensity of all the tested areas using ImageJ. Then, the detection concentration of each sample was obtained based on Hill's equation previously fitted. The detection concentration values for each sample are listed in Table S3. Among them, 4 out of 19 healthy samples were detected as unhealthy samples, implying that the concentrations of their test results were higher than the cut-off value of plasma Aβ 1-42 concentration (16.42 pg mL-1 [16]). Meanwhile, 1 out of 19 unhealthy samples was detected as a healthy sample. The results are shown in Fig. 5b. Thus, we obtained an accuracy of 86.84% ((15 detected healthy samples + 18 detected unhealthy samples)/38 total samples) using the conventional analysis method.

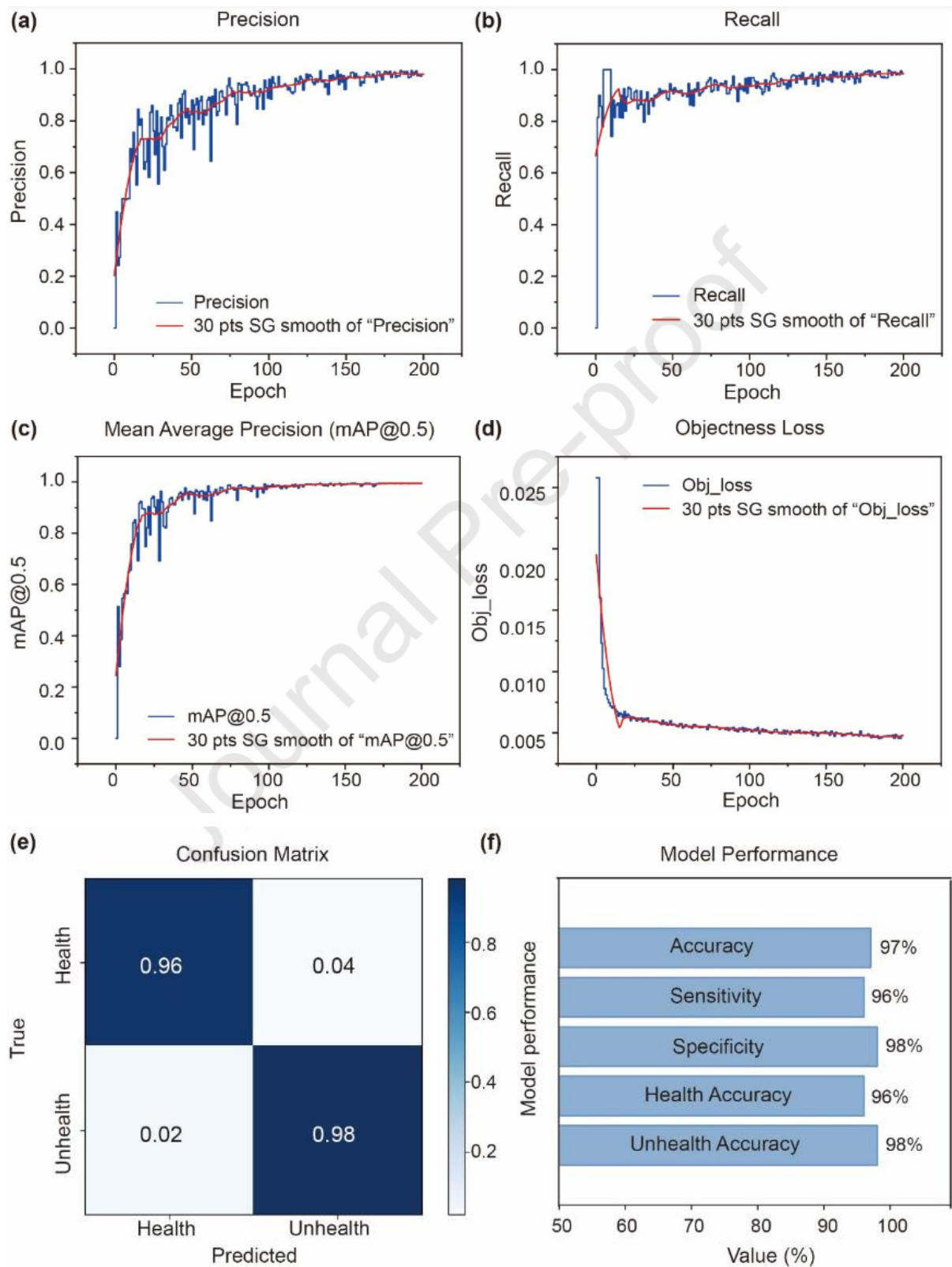The training results of the YOLOv5 model (The performance of YOLOv5 model)

Fig. 6. The training results of the YOLOv5 model. (a) The target detection accuracy (Precision), and (b) Target detection recall. (c) The mean average precision at 0.5 (mAP@0.5). (d) The objectless loss. (e) The confusion matrix. (f) The model performance.

In this work, the performance of the YOLOv5 model is comprehensively evaluated in terms of precision, recall, mean average precision (mAP), objectless loss, accuracy, specificity, and sensitivity. Before describing the individual performance specifically, it is necessary to realize that the true positive (TP) means the sensor (smartphone-based platform) correctly predicts a positive (healthy) classification of the sample. The false positive (FP) is defined as the sensor incorrectly determining the negative sample (unhealthy sample) to be the positive (healthy) one. The true negative (TN) and false negative (FN) follow the same. Typically, the training results of the YOLOv5 model can also be evaluated by visualizing the training results. The main observation is the fluctuation of precision and recall, and the fluctuation is not large means the training result is relatively satisfactory. Fig. 6(a) shows that the precision stabilizes after the 150th epoch (training round). Higher precision means a lower probability that an unhealthy sample is predicted to be a healthy sample, which can be expressed by Eq. 1. Further, a precision-confidence curve (as shown in Fig. S3) represents the recognition precision of each class when the confidence is set to a certain value. As the confidence increases, the classes are detected more precisely.

Recall is used to describe how many real healthy samples are predicted, which is equivalent to the sensitivity of the YOLOv5 model and can be expressed by Eq. 2. Fig. 6(b) illustrates that the recall produces a substantial boost at the 10th epoch, and then gradually stabilizes. Higher recall means fewer healthy samples are predicted to be unhealthy. The recall-confidence curve indicates that the high recall rate confirms the effectiveness of the model in real detection tasks (as shown in Fig. S4). In addition, the precision-recall curve (as shown in Fig. S5) is a comprehensive evaluation tool that illustrates the balance between precision and recall for various confidence thresholds set for model predictions. An equilibrium model with high precision and recall ensures accurate identification of detections. When the precision-recall curves show consistently high precision and recall values at different confidence thresholds, it indicates that the YOLOv5 model performs well in the detection task.

Moreover, the F1-confidence curve (as shown in Fig. S6) is a useful metric for evaluating the overall performance of the YOLOv5 model by combining precision and recall into a single metric (as shown in Eq. 3). The F1 score is a balanced metric for evaluating the performance of the model because it considers both precision and recall.

$$Precision = TP/(TP + FP) \quad (1)$$

$$Recall = Sensitivity = TP/(TP + FN) \quad (2)$$

$$F1\ score = (2*(Precision*Recall))/(Precision + Recall) \quad (3)$$

Fig. 6(c) shows the gradual stabilization of mean Average Precision at IoU 0.5 (mAP@0.5) after the 75th epoch. mAP@0.5 is a commonly used target detection evaluation metric to measure the average accuracy of a model over different categories. It is calculated involving Precision and Recall. mAP@0.5 specifically refers to the mAP value at an Intersection over the Union (IoU) threshold of 0.5. IoU is used to measure the degree of overlap between the predicted bounding box and the true target bounding box. The prediction is considered correct when the IoU between the predicted bounding box and the true target bounding box is greater than or equal to 0.5. Therefore, mAP@0.5 represents the average accuracy of the model under an IoU threshold of 0.5. It considers the Precision and Recall of the model on different categories and takes their average as the final evaluation result. Meanwhile, higher mAP@0.5 values indicate that the model performs better in the target detection task, detects the target more accurately, and obtains a lower false detection rate. Objective loss (Fig. 6 (d)) is the loss function used to train the deep learning model and is used to measure the difference between the model predictions and the true labels. The objective loss function is designed to minimize the prediction error of the model so that the model can better fit the training data and gradually optimize the parameters of the model during the training process. By optimizing the target loss, the model can gradually improve its performance in the target detection task and increase the accuracy and precision of target detection. The above four values are the commonly used evaluation parameters for the YOLOv5 model.

In addition, to further evaluate the YOLOv5 model, we analyzed its corresponding confusion matrix image (as shown in Fig. 6(e)). From the confusion matrix we can get the value of TP is 0.96, the FN is 0.04, the FP is 0.02, and the TN is 0.98. Accuracy is a measurement used to indicate the accuracy of a classification model in the prediction process. It represents the ratio between the number of samples correctly predicted by the model and the total number of samples (as shown in Eq. 3). A higher accuracy rate indicates that the model has better classification ability and can assign samples to the correct category more accurately. Moreover, accuracy is usually widely used in the context of classification balance. Here, the value of accuracy can be calculated as 97%.

$$Accuracy = (TP + TN)/(TP + FP + TN + FN) \quad (3)$$

Specificity is the ability of a classification model to correctly predict negative class samples (true negative samples). It is a measure of the accuracy of the model in identifying negative class samples. Specifically, the specificity can be calculated by Eq. 4 (The value is 98%). A model with high specificity means that it is effective in classifying negative class samples correctly and reduces the probability of misclassifying negative class samples as positive classes. It is important to note that specificity and sensitivity (recall) are complementary metrics. Sensitivity measures the ability of a model to correctly

predict in a positive class of samples, while specificity focuses on correct prediction in a negative class of samples. When evaluating model performance, we usually need to consider the results of specificity, sensitivity, and other metrics together to get a full picture of the classification of model ability. Based on the results of the parameters we obtained (as in Fig. 6(f)), the YOLOv5 model provides promising training results for our dataset.

$$Specificity = TN/(TN+FP) \qquad (4)$$

Although there are many metrics for evaluating models, the evaluation of models must consider multiple metrics for thorough testing to verify the validity of the model in real-world situations. The training environment configuration and the training parameter setting of detection model information can be found in Table S4 and S5.

Android application

An NCNN framework provided by Tencent as a high-performance neural network forward computing framework can port the deep learning models generated on the computer to the smartphone. Therefore, in this work, we transfer the YOLOv5 model to the smartphone using the NCNN framework to achieve offline detection. Moreover, the Android system smartphone has the advantages of low development cost and high versatility (>70% market share worldwide) [49]. Therefore, we developed an Android application with simple and user-friendly interfaces capable of controlling servo motor rotation via Bluetooth, and automatically performing image processing and result analysis, further providing a more convenient platform for data analysis. Specifically, the user logs into the interface and selects the project to be tested. After clicking the start button, the user connects to the Arduino control board via Bluetooth, if the connection is successful, the user continues to click the start button, and the sandwich c-ELISA test will be performed according to the pre-programmed protocol. At the end of the test, the sandwich c-ELISA results will be obtained through the smartphone camera and analyzed. The result (healthy/unhealthy) will be displayed on the screen.

Conclusion

This paper presents a smartphone-based automatic μPAD platform featuring a highly integrated rotary valve with deep learning-assisted highly accurate offline detection for AD. We utilize a simple mechanical rotary structure with signal transmission between a smartphone and a Bluetooth module to achieve a simple, highly integrated, and highly stable fully automated c-ELISA assay. The key is that this paper realizes offline detection of smartphones, avoiding the need for large-scale computing devices and data transmission in the cloud, and can implement real-time monitoring and rapid detection even in areas with poorly developed communications. Specifically, to construct the deep

learning model training dataset, we first simulated 38 artificial plasma Aβ 1-42 samples with 19 healthy samples and 19 unhealthy samples. After performing the sandwich c-ELISA detection six times (N=6) for each sample using a smartphone-based automatic μPAD platform, we used eight different smartphones to capture the detection results (to improve the robustness and adaptability of the deep learning algorithms) and ultimately collected 1824 results images (38 samples $\subseteq$ 6 times $\subseteq$ 8 smartphones=1824 images). Then, the YOLOv5 deep learning model was used to train the dataset, obtaining an accuracy of 97%, which is 10.16% higher than the conventional curve-fitting results analysis method, and it also provides an average accuracy (mAP) of 99.45%. Finally, we utilize the NCNN framework provided by Tencent to deploy YOLOv5 deep learning model directly to smartphones for offline local detection. Furthermore, we developed a userfriendly smartphone APP to control the whole assay process. The unique capabilities of our platform further enhance the advantages of μPAD for universal use in lowresource settings and offer great potential and opportunities for the development of POCT. At the same time, it provides a feasible approach for effective AD detection on a large scale.

CRediT authorship contribution statement

Sixuan Duan: Conceptualization, Methodology, Software, Writing-Original Draft, Writing-Reviewing and Editing. Tianyu Cai: Methodology, Validation. Fuyuan Liu: Visualization. Yifan Li: Data Curation. Hang Yuan: Visualization. Wenwen Yuan: Visualization. Kaizhu Huang: Supervision. Kai Hoettges: Supervision. Min Chen: Supervision. Eng Gee Lim: Supervision. Chun Zhao: Supervision. Pengfei Song: Conceptualization, Writing-Reviewing and Editing, Supervision.

Declaration of competing interest The authors declare that they have no known competing financial interests or personal relationships that could have appeared to influence the work reported in this paper.

References

[1] A. Leuzy, N. Mattsson-Carlgren, S. Palmqvist, S. Janelidze, J.L. Dage, O. Hansson, Blood - based biomarkers for Alzheimer's disease, EMBO molecular medicine, 14 (2022) e14408.

[2] H. Zetterberg, J.M. Schott, Blood biomarkers for Alzheimer's disease and related disorders, Acta Neurologica Scandinavica, 146 (2022) 51-55.

[3] C. Laske, H.R. Sohrabi, S.M. Frost, K. López-de-Ipiña, P. Garrard, M. Buscema, J. Dauwels, S.R. Soekadar, S. Mueller, C. Linnemann, Innovative diagnostic tools for early detection of Alzheimer's disease, Alzheimer's & Dementia, 11 (2015) 561-578.

[4] P. Schneider, H. Hampel, K. Buerger, Biological marker candidates of Alzheimer's disease in blood, plasma, and serum, CNS neuroscience & therapeutics, 15 (2009) 358-374.

[5] S.-S. Li, C.-W. Lin, K.-C. Wei, C.-Y. Huang, P.-H. Hsu, H.-L. Liu, Y.-J. Lu, S.-C. Lin, H.-W. Yang, C.-C.M. Ma, Non-invasive screening for early Alzheimer's disease diagnosis by a sensitively immunomagnetic biosensor, Scientific reports, 6 (2016) 25155.

[6] J. Dukart, K. Mueller, H. Barthel, A. Villringer, O. Sabri, M.L. Schroeter, A.s.D.N. Initiative, Meta-analysis based SVM classification enables accurate detection of Alzheimer's disease across different clinical centers using FDG-PET and MRI, Psychiatry Research: Neuroimaging, 212 (2013) 230-236.

[7] O. Sabri, M.N. Sabbagh, J. Seibyl, H. Barthel, H. Akatsu, Y. Ouchi, K. Senda, S. Murayama, K. Ishii, M. Takao, Florbetaben PET imaging to detect amyloid beta plaques in Alzheimer's disease: phase 3 study, Alzheimer's & dementia, 11 (2015) 964-974.

[8] L. Mosconi, M. Brys, L. Glodzik-Sobanska, S. De Santi, H. Rusinek, M.J. De Leon, Early detection of Alzheimer's disease using neuroimaging, Experimental gerontology, 42 (2007) 129-138.

[9] K. Blennow, B. Dubois, A.M. Fagan, P. Lewczuk, M.J. De Leon, H. Hampel, Clinical utility of cerebrospinal fluid biomarkers in the diagnosis of early Alzheimer's disease, Alzheimer's & Dementia, 11 (2015) 58-69.

[10] M. Bjerke, S. Engelborghs, Cerebrospinal fluid biomarkers for early and differential Alzheimer's disease diagnosis, Journal of Alzheimer's Disease, 62 (2018) 1199-1209.

[11] M. Sjögren, N. Andreasen, K. Blennow, Advances in the detection of Alzheimer's disease—use of cerebrospinal fluid biomarkers, Clinica Chimica Acta, 332 (2003) 1- 10.

[12] S. Hu, C. Yang, H. Luo, Current trends in blood biomarker detection and imaging for Alzheimer's disease, Biosensors and Bioelectronics, 210 (2022) 114278.

[13] S.E. O'Bryant, G. Xiao, R. Barber, J. Reisch, J. Hall, C.M. Cullum, R. Doody, T. Fairchild, P. Adams, K. Wilhelmsen, A blood-based algorithm for the detection of Alzheimer's disease, Dementia and geriatric cognitive disorders, 32 (2011) 55-62.

[14] A. Nabers, L. Perna, J. Lange, U. Mons, J. Schartner, J. Güldenhaupt, K.U. Saum, S. Janelidze, B. Holleczek, D. Rujescu, Amyloid blood biomarker detects Alzheimer's disease, EMBO molecular medicine, 10 (2018) e8763.

[15] C.E. Teunissen, M.-J. Chiu, C.-C. Yang, S.-Y. Yang, P. Scheltens, H. Zetterberg, K. Blennow, Plasma amyloid-β (Aβ 42) correlates with cerebrospinal fluid Aβ 42 in Alzheimer's disease, Journal of Alzheimer's Disease, 62 (2018) 1857-1863.

[16] S.-Y. Yang, M.-J. Chiu, T.-F. Chen, H.-E. Horng, Detection of plasma biomarkers using immunomagnetic reduction: a promising method for the early diagnosis of Alzheimer's disease, Neurology and therapy, 6 (2017) 37-56.

[17] V. Ovod, K.N. Ramsey, K.G. Mawuenyega, J.G. Bollinger, T. Hicks, T. Schneider, M. Sullivan, K. Paumier, D.M. Holtzman, J.C. Morris, Amyloid β concentrations and stable isotope labeling kinetics of human plasma specific to central nervous system amyloidosis, Alzheimer's & Dementia, 13 (2017) 841-849.

[18] H. Fu, P. Song, Q. Wu, C. Zhao, P. Pan, X. Li, N.Y. Li-Jessen, X. Liu, A paperbased microfluidic platform with shape-memory-polymer-actuated fluid valves for automated multi-step immunoassays, Microsystems & nanoengineering, 5 (2019) 50.

[19] S. Ghosh, K. Aggarwal, V.T. U, T. Nguyen, J. Han, C.H. Ahn, A new microchannel capillary flow assay (MCFA) platform with lyophilized chemiluminescence reagents for a smartphone-based POCT detecting malaria, Microsystems & Nanoengineering, 6 (2020) 5.

[20] Q. Song, X. Sun, Z. Dai, Y. Gao, X. Gong, B. Zhou, J. Wu, W. Wen, Point-ofcare testing detection methods for COVID-19, Lab on a Chip, 21 (2021) 1634-1660.

[21] T. Tian, X. Wei, S. Jia, R. Zhang, J. Li, Z. Zhu, H. Zhang, Y. Ma, Z. Lin, C.J. Yang, Integration of target responsive hydrogel with cascaded enzymatic reactions and microfluidic paper-based analytic devices (μPADs) for point-of-care testing (POCT), Biosensors and Bioelectronics, 77 (2016) 537-542.

[22] R. Ghosh, S. Gopalakrishnan, R. Savitha, T. Renganathan, S. Pushpavanam, Fabrication of laser printed microfluidic paper-based analytical devices (LP-μPADs) for point-of-care applications, Scientific Reports, 9 (2019) 7896.

[23] T. Tian, Y. Bi, X. Xu, Z. Zhu, C. Yang, Integrated paper-based microfluidic devices for point-of-care testing, Analytical methods, 10 (2018) 3567-3581.

[24] X. Li, Z. Qin, H. Fu, T. Li, R. Peng, Z. Li, J.M. Rini, X. Liu, Enhancing the performance of paper-based electrochemical impedance spectroscopy nanobiosensors: An experimental approach, Biosensors and Bioelectronics, 177 (2021) 112672.

[25] S. Wang, L. Ge, X. Song, J. Yu, S. Ge, J. Huang, F. Zeng, based chemiluminescence ELISA: lab-on-paper based on chitosan modified paper device and wax-screen-printing, Biosensors and bioelectronics, 31 (2012) 212-218.

[26] R.V. Taudte, A. Beavis, L. Wilson-Wilde, C. Roux, P. Doble, L. Blanes, A portable explosive detector based on fluorescence quenching of pyrene deposited on coloured wax-printed μPADs, Lab on a Chip, 13 (2013) 4164-4172.

[27] S. Duan, T. Cai, J. Zhu, X. Yang, E.G. Lim, K. Huang, K. Hoettges, Q. Zhang, H. Fu, Q. Guo, Deep learning-assisted ultra-accurate smartphone testing of paper-based colorimetric ELISA assays, Analytica Chimica Acta, 1248 (2023) 340868.

[28] S. Cheng, J. Sun, J. Yang, J. Lv, F. Wu, Y. Lin, L. Liao, Y. Ye, C. Cao, L. Fang, A new immunoassay of serum antibodies against Peste des petits ruminants virus using quantum dots and a lateral-flow test strip, Analytical and bioanalytical chemistry, 409 (2017) 133-141.

[29] A. Kumar, D. Jain, J. Bahuguna, M. Bhaiyya, S.K. Dubey, A. Javed, S. Goel, Machine learning assisted and smartphone integrated homogeneous electrochemiluminescence biosensor platform for sample to answer detection of various human metabolites, Biosensors and Bioelectronics, 238 (2023) 115582.

[30] J. Liu, Z. Geng, Z. Fan, J. Liu, H. Chen, Point-of-care testing based on smartphone: The current state-of-the-art (2017–2018), Biosensors and Bioelectronics, 132 (2019) 17-37.

[31] H.-A. Joung, Z.S. Ballard, J. Wu, D.K. Tseng, H. Teshome, L. Zhang, E.J. Horn, P.M. Arnaboldi, R.J. Dattwyler, O.B. Garner, Point-of-care serodiagnostic test for early-stage Lyme disease using a multiplexed paper-based immunoassay and machine learning, ACS nano, 14 (2019) 229-240.

[32] Q. Ning, W. Zheng, H. Xu, A. Zhu, T. Li, Y. Cheng, S. Feng, L. Wang, D. Cui, K. Wang, Rapid segmentation and sensitive analysis of CRP with paper-based microfluidic device using machine learning, Analytical and Bioanalytical Chemistry, 414 (2022) 3959-3970.

[33] X. Guo, M.A. Khalid, I. Domingos, A.L. Michala, M. Adriko, C. Rowel, D. Ajambo, A. Garrett, S. Kar, X. Yan, Smartphone-based DNA diagnostics for malaria detection using deep learning for local decision support and blockchain technology for security, Nature Electronics, 4 (2021) 615-624.

[34] S. Tuli, S. Tuli, R. Tuli, S.S. Gill, Predicting the growth and trend of COVID-19 pandemic using machine learning and cloud computing, Internet of Things, 11 (2020) 100222.

[35] R. Zenhausern, A.S. Day, B. Safavinia, S. Han, P.E. Rudy, Y.-W. Won, J.-Y. Yoon, Natural killer cell detection, quantification, and subpopulation identification on paper microfluidic cell chromatography using smartphone-based machine learning classification, Biosensors and Bioelectronics, 200 (2022) 113916.

[36] F. Cui, Y. Yue, Y. Zhang, Z. Zhang, H.S. Zhou, Advancing biosensors with machine learning, ACS sensors, 5 (2020) 3346-3364.

[37] K. Zhang, J. Wang, T. Liu, Y. Luo, X.J. Loh, X. Chen, Machine learning- reinforced noninvasive biosensors for healthcare, Advanced Healthcare Materials, 10 (2021) 2100734.

[38] O.D. Incel, S.Ö. Bursa, On-device deep learning for mobile and wearable sensing applications: A review, IEEE Sensors Journal, 23 (2023) 5501-5512.

[39] H. Zhang, E. Smith, W. Zhang, A. Zhou, Inkjet printed microfluidic paper-based analytical device (μPAD) for glucose colorimetric detection in artificial urine, Biomedical microdevices, 21 (2019) 1-10.

[40] Y. Chen, J. Sun, Y. Xianyu, B. Yin, Y. Niu, S. Wang, F. Cao, X. Zhang, Y. Wang, X. Jiang, A dual-readout chemiluminescent-gold lateral flow test for multiplex and ultrasensitive detection of disease biomarkers in real samples, Nanoscale, 8 (2016) 15205-15212.

[41] M. Chiriboga, C.M. Green, D.A. Hastman, D. Mathur, Q. Wei, S.A. Díaz, I.L. Medintz, R. Veneziano, Rapid DNA origami nanostructure detection and classification using the YOLOv5 deep convolutional neural network, Scientific Reports, 12 (2022) 3871.

[42] T.B. Pun, A. Neupane, R. Koech, K. Walsh, Detection and counting of root-knot nematodes using YOLO models with mosaic augmentation, Biosensors and Bioelectronics: X, 15 (2023) 100407.

[43] T. Zeng, S. Li, Q. Song, F. Zhong, X. Wei, Lightweight tomato real-time detection method based on improved YOLO and mobile deployment, Computers and Electronics in Agriculture, 205 (2023) 107625.

[44] T. Cai, S. Duan, H. Fu, J. Zhu, E.G. Lim, K. Huang, K. Hoettges, X. Liu, P. Song, A Paper-Based Microfluidic Analytical Device with A Highly Integrated On-Chip Valve For Autonomous ELISA, 2022

IEEE 35th International Conference on Micro Electro Mechanical Systems Conference (MEMS), IEEE, 2022, pp. 271-274.

[45] R. Liu, C. Ren, M. Fu, Z. Chu, J. Guo, Platelet detection based on improved yolo_v3, Cyborg and Bionic Systems, 2022 (2022).

[46] G. Zhan, W. Wang, H. Sun, Y. Hou, L. Feng, Auto-csc: a transfer learning based automatic cell segmentation and count framework, Cyborg and Bionic Systems, 2022 (2022).

[47] J. Luo, H. Long, W. Sheng, H. Hui, R. Li, T. Yan, Residential Solar Panel Object Detection Based on Multi-combination Data Augmentation and YOLOv5, 2023 IEEE 6th International Electrical and Energy Conference (CIEEC), IEEE, 2023, pp. 2117- 2122.

[48] H. Bayer, A. Aziz, Object detection of fire safety equipment in images and videos using Yolov5 neural network, Proceedings of 33. Forum Bauinformatik, 2022.

[49] Q. Fu, C. Zhang, J. Xie, Z. Li, L. Qu, X. Cai, H. Ouyang, Y. Song, D. Du, Y. Lin, Ambient light sensor based colorimetric dipstick reader for rapid monitoring organophosphate pesticides on a smart phone, Analytica Chimica Acta, 1092 (2019) 126-131.